To be submitted to
Nuclear Instruments
and Methods

ISTITUTO NAZIONALE DI FISICA NUCLEARE
Laboratori Nazionali di Frascati

LNF-82/32(P)
11 Maggio 1982

H. Bilokon, G. Bologna, F. Celani, B. D'Ettorre Piazzoli, R. Falcioni, G. Mannocchi and P. Picchi: COHERENT BREMSSTRAHLUNG IN CRYSTALS AS A TOOL FOR PRODUCING HIGH ENERGY PHOTON BEAMS TO BE USED IN PHOTOPRODUCTION EXPERIMENTS AT CERN SPS

Servizio Documentazione
dei Laboratori Nazionali di Frascati
Cas. Postale 13 - Frascati (Roma)

INFN - Laboratori Nazionali di Frascati
Servizio Documentazione

LNF-82/32(P)
11 Maggio 1982

COHERENT BREMSSTRAHLUNG IN CRYSTALS AS A TOOL FOR PRODUCING HIGH ENERGY PHOTON BEAMS TO BE USED IN PHOTOPRODUCTION EXPERIMENTS AT CERN SPS

F. Celani, R. Falcioni
INFN - Laboratori Nazionali di Frascati

H. Bilokon, B. D'Ettorre Piazzoli, G. Mannocchi
Istituto di Cosmogeofisica del CNR, Torino, and INFN - Laboratori Nazionali di Frascati

G. Bologna, P. Picchi
Istituto di Fisica Generale dell'Università di Torino, Istituto di Cosmogeofisica del CNR, Torino, and INFN - Laboratori Nazionali di Frascati.

ABSTRACT

We recall the properties of coherent bremsstrahlung of high energy electrons in single crystals and show that a suitably oriented diamond crystal can produce a high energy bremsstrahlung beam whose quasi-monochromatic spectral composition may be exploited for increasing the production rate in a phtoproduction experiment at hundreds of GeV. A careful analysis of the required angular resolutions is performed. It turns out that the standard deviation of the electron beam angular divergence in one plane should be less than 0.3 mrad, for a beam energy of 150 GeV. The standard deviation in the perpendicular plane is not critical. In this situation the photoproduction rate in a typical case is increased by a factor of about 3 with respect to the conventional bremsstrahlung beam.

1. - INTRODUCTION

We discuss the characteristics of the coherent bremsstrahlung process which could help in improving the quality of the photon beam used by experiment NA1[1] at CERN Super Proton Synchrotron (SPS). However our considerations are sufficiently general to be useful for any other similar bremsstrahlung beam.

Experimental investigation of coherent bremsstrahlung and pair production processes in crystals has been carried out at practically all the high energy electron accelerator laboratories. Accounts of this work can be found in several review papers[2] or books[3]. Among proton accelerators, the Serpukov Proton Synchrotron is the only one which has a coherent bremsstrahlung beam[4]. Applications to CERN SPS[5, 6] and FNAL[7] beams as well as future CERN LEP physics[8] have been also proposed.

Interest in using coherent bremsstrahlung in photoproduction experiments stems from two particular features: a) its degree of monochromaticity; b) its degree of polarization.

In what follows we focus our attention mainly on point a) because this is the feature which at present interests us. On the other hand, point b) is less attractive in the foreseen experimental situation: it turns out that the linear polarization is rather poor (see Sect. 7).

2. - THE PROCESS OF COHERENT BREMSSTRAHLUNG - QUALITATIVE ACCOUNT

We now simply recall the essential features of coherent bremsstrahlung in crystals without giving many details. See ref. (2) and (3) for a full account. A review paper[9] concerning the bremsstrahlung process in general (i. e. : not in crystals) may also be useful. Our notation and units will be as close as possible to those used in this work.

Let us define:

m_o electron rest mass;

h Plank's constant;

c velocity of light in vacuum;

λ_o $= h/m_o c$ Compton wave length of the electron;

$\vec{p}_o$ primary electron momentum in $m_o c$ units;

E_o primary electron energy in $m_o c^2$ units;

k photon energy in $m_o c^2$ units;

x $= k/E_o$ photon fractional energy;

$\vec{q}$ recoil momentum of the crystal in $m_o c$ units;

q_z component of $\vec{q}$ along $\vec{p}_o$;

q_t component of $\vec{q}$ perpendicular to $\vec{p}_o$;

δ minimum recoil momentum in $m_o c$ units;

$\vec{a}_1, \vec{a}_2, \vec{a}_3$ direct lattice axes (magnitudes in λ_o Compton units);

$\vec{b}_1, \vec{b}_2, \vec{b}_3$ reciprocal lattice axes;

$\vec{\xi}_1, \vec{\xi}_2, \vec{\xi}_3$ actual reference axes;

$\vec{g}$ reciprocal lattice vector;

θ $= \sphericalangle(\vec{\xi}_1, \vec{p}_o)$ electron polar angle in units of $1/E_o$;

α $= \sphericalangle(\vec{\xi}_1, \vec{p}_o)(\vec{\xi}_1, \vec{\xi}_2)$ electron azimuthal angle in degrees;

Z atomic number.

When conventional units are used, the corresponding quantity is cupped. Thus, for instance, E_o is the electron energy in $m_o c^2$ units and $\breve{E}_o$ is the same quantity in MeV, and $\breve{E}_o = m_o c^2 E_o$.

When a high ($> \sim 200$ MeV) energy primary (electron or photon) strikes a single crystal, interference effects occur in the interaction (bremsstrahlung or pair production), much in the same way as in the case of X-ray scattering. This looks like a paradox, as in the present case the incoming particle wave length is much less than the crystal lattice spacing, so the Bragg condition can't be satisfied. However, the essence of coherent X-ray scattering in a crystal is that the crystal recoils as a whole with a momentum $\vec{q}$ which is equal to a reciprocal lattice vector $\vec{g}$ (Laue condition).

Now, high energy bremsstrahlung ($E_o \gg 1$) and pair production ($k \gg 1$) are processes in which the recoil momentum $\vec{q}$ is very small: it has a transverse component $q_t < \sim 1$ and a longitudinal component $\delta < q_z < \sim 2\delta$, where

$$\delta = \frac{1}{2E_o} \frac{x}{1-x} \tag{1}$$

is the minimum recoil momentum for bremsstrahlung (we don't consider pair production any longer in this paper).

This means that:

a) The Laue condition $\vec{q} = \vec{g}$ can still be satisfied ($g \sim 10^{-2}$ for typical crystals).

b) The formation zone of the bremsstrahlung along the electron direction, which, according to the uncertainty principle, is $\propto 1/q_z$, can include many periodically located atoms. Amplitudes from all these atoms sum up coherently, so that the cross section per atom is proportional to the number of coherently acting atoms.

The previous kinematical description can also be displayed graphically. Fig. 1 shows the reciprocal lattice space of a diamond crystal. The momentum $\vec{p}_o$ makes an angle θ with the axis $\vec{\zeta}_1$ while α is the angle of the planes $(\vec{\zeta}_1, \vec{p}_o)$ and $(\vec{\zeta}_1, \vec{\zeta}_2)$. The kinematically allowed region for the recoil momentum of the crystal has the shape of a pancake orthogonal to $\vec{p}_o$, having a sharp distance δ from the origin of the reciprocal lattice space, a smooth thickness δ and a smooth radius equal to 1. In Fig. 1 the intersection of the pancake surfaces with the reference lattice planes are drawn. The shaded area represents the intersection of the pancake with the plane $(\vec{\zeta}_2, \vec{\zeta}_3)$.

As the Laue condition holds for coherent bremsstrahlung, the cross-section takes contributions only

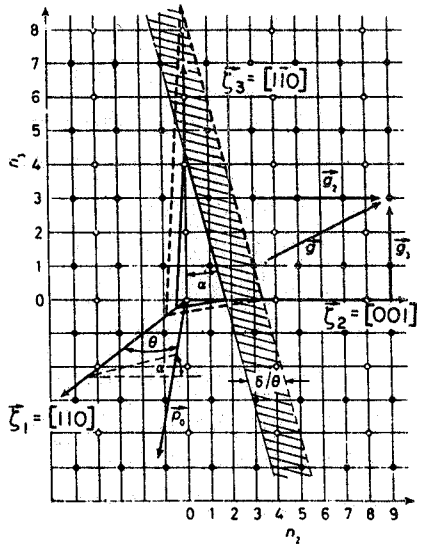

FIG. 1 - Reciprocal lattice space of the diamond crystal.

from those reciprocal lattice points which are inside the pancake. Furthermore, the contribution to the cross section is essentially different from zero only for those reciprocal lattice points which lie in the plane $(\vec{\zeta}_2, \vec{\zeta}_3)$ through the origin.

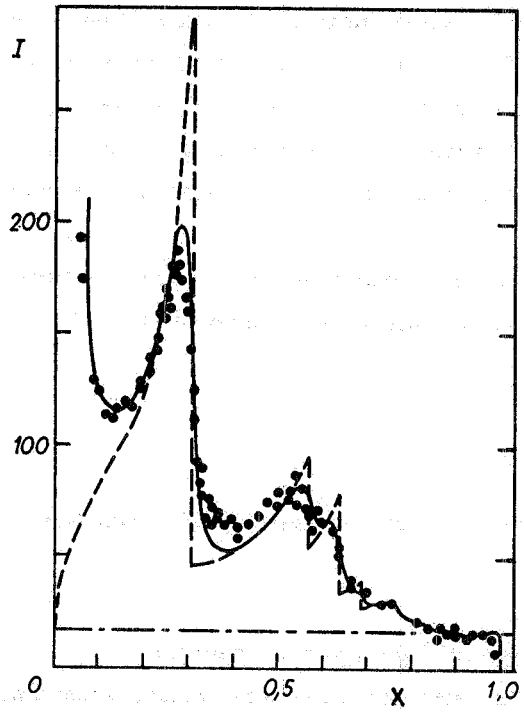

FIG. 2 - Bremsstrahlung intensity versus $x = k/E_o$ for diamond. Axes as in Fig. 1. $\breve{E}_o = 4.8$ GeV ; $\breve{\theta} = 3.44$ mrad ; $\alpha = 0$.

By changing θ and/or k and/or E_o the pancake sweeps the points of the lattice. Correspondingly the shaded area of Fig. 1 moves across the points of the plane $(\vec{\zeta}_2, \vec{\zeta}_3)$. Every time it includes or excludes a point on the left side, a sharp discontinuity is produced in the cross-section.

In Fig. 2 (taken from ref. (10)), the bremsstrahlung intensity for a diamond single crystal, $I(x) = k dN/dk$, is represented, in arbitrary units, versus x ; dN is the number of photons in the range dk at k. Other parameters are: $\breve{E}_o = 4.8$ GeV, $\breve{\theta} = 3.44$ mrad, $\alpha = 0$. Reference axes are the same as in Fig. 1.

The dashed curve is obtained for an ideal situation in which the primary electron beam enters the crystal without any divergence and suffers no multiple scattering. The discontinuous behaviour of this curve confirms the qualitative picture given above. Now the shaded area in Fig. 1 is vertical ($\alpha = 0$) and an entire row of points escapes the pancake at a time, giving discontinuities at $x = 0.3$, etc.

The continous curve has been obtained by making allowance for 1 mrad electron natural spread, and 1 mm thickness multiple scattering. It is in remarkable agreement with the experimental results, represented by the dots.

When x approaches zero (and so does δ), there are no points of the lattice within the pancake ; thus the coherent cross section vanishes in the "ideal" situation (however, the dashed curve does not reach zero at $x = 0$, due to the presence of an incoherent thermal background of the Bethe-Heitler type, which is represented by the dot-dashed curve).

In the actual experimental conditions, the direction of $\vec{p}_o$ has a range of values within a cone. Thus also α has a range of values and the pancake intersection in Fig. 1 includes the point $n_3 = 2$ on the axis $\vec{\zeta}_3$, for which the contribution to the cross section is largest. Correspondingly, the continuous curve has a steep rise for x approching 0.

3. - THE COHERENT BREMSSTRAHLUNG CROSS SECTION

We now discuss the process from a quantitative point of view. What we need is essentially a γ-ray beam which is monochromatic as far as possible. The extent to which coherent bremsstrahlung can be monochromatized by collimation of the photon beam has been discussed in ref. (11). The effect is feasible in the GeV region, but is inapplicable at SPS energies and electron fluxes. Thus we have to rely on the entire bremsstrahlung cone.

We give the expression for the cross section integrated over angles, and differential in photon energy for crystals of the elements and in the following hypotheses[9]:

a) Born approximation (See Sect. 4);

b) Extreme relativistic (E_o, $E_o - k$, $k \gg 1$);

c) Complete screening ($137\, Z^{-1/3} \delta \ll 1$).

The cross section per atom is given by the following expression[11]:

$$d\sigma = \bar{\sigma} I(x, E_o, \theta, a) \frac{dx}{x} \; ; \quad \bar{\sigma} = \frac{Z^2}{137} \left(\frac{e^2}{m_o c^2}\right)^2 = 58 \cdot Z^2 \text{ mbarn} \; ;$$
$$I(x, E_o, \theta, a) = I_i(x, E_o, \theta, a) + I_c(x, E_o) \; . \tag{2}$$

$$I_i(x, E_o, \theta, a) = \frac{E_o}{D} \left\{ \left[1+(1-x)^2\right] \chi_1\left(\frac{\theta}{D}, a\right) - \frac{2}{3}(1-x)\, \chi_2\left(\frac{\theta}{D}, a\right) \right\} \; ;$$
$$D = \delta E_o = \frac{x}{2(1-x)} \; . \tag{3}$$

$$\chi_1\left(\frac{\theta}{D}, a\right) = \sum_{\vec{g}} \frac{\phi(\vec{g})}{\xi^2} \; ; \quad \chi_2\left(\frac{\theta}{D}, a\right) = 6 \sum_{\vec{g}} \phi(\vec{g}) \frac{\xi - 1}{\xi^4} \; ; \quad \xi = \frac{q_z}{\delta} \; . \tag{4}$$

$$\phi(\vec{g}) = \frac{2|S|^2}{\pi V n} \frac{\left[1 - F(g^2)\right]^2}{g^2} e^{-A g^2} \; ; \quad S = \sum_{j=1}^{n} \exp\left[2\pi i (\ell_1 u_{1j} + \ell_2 u_{2j} + \ell_3 u_{3j})\right] \tag{5}$$

$$I_c(x, E_o) = \left[1+(1-x^2)\right] \psi_1^c - \frac{2}{3}(1-x)\, \psi_2^c \; ; \quad \psi_1^c = 2(2 \cdot \ln\beta + T + 2) \; ; \quad \psi_2^c = \psi_1^c - \frac{2}{3} \; ;$$
$$\beta = 111 \cdot Z^{1/3} \; ; \quad T = \left(1 + \frac{A}{\beta^2}\right) e^{\frac{A}{\beta^2}} \, Ei\left(-\frac{A}{\beta^2}\right) \; ; \quad Ei(-v) = -\int_v^{\infty} \frac{e^{-t}}{t} dt \; . \tag{6}$$

In eqs. (5), $F(g^2)$ (i.e. : $F(q^2)$) represents the atomic electron form factor[9]. A is the Debey-Waller thermal factor, which is a measure of the mean square displacement of an atom from its equilibrium position in the crystal lattice. If $\vec{a}_1$, $\vec{a}_2$, $\vec{a}_3$ are the direct lattice axes, $V = \vec{a}_1 x \vec{a}_2 \cdot \vec{a}_3$ expresses the volume of the basis lattice cell, which contains n atoms at positions u_{1j}, u_{2j}, u_{3j} ($j = 1, 2, \ldots, n$), expressed as fractions of the sides $|\vec{a}_1|$, $|\vec{a}_2|$, $|\vec{a}_3|$ of the cell.

In eqs. (5), the triplet of integers ℓ_1, ℓ_2, ℓ_3 (negative values are indicated by a bar above the integer) specifies a reciprocal lattice vector $\vec{g}$, as defined with respect to the reciprocal lattice axes $\vec{b}_1, \vec{b}_2, \vec{b}_3$, where

$$\vec{b}_1 = \frac{\vec{a}_2 \times \vec{a}_3}{V} \; ; \qquad \vec{b}_2 = \frac{\vec{a}_3 \times \vec{a}_1}{V} \; ; \qquad \vec{b}_3 = \frac{\vec{a}_1 \times \vec{a}_2}{V} \; .$$

In this frame, $\vec{g} = \vec{g}_1 + \vec{g}_2 + \vec{g}_3$ is represented by

$$\vec{g}_1 = \ell_1 \vec{b}_1 \; ; \qquad \vec{g}_2 = \ell_2 \vec{b}_2 \; ; \qquad \vec{g}_3 = \ell_3 \vec{b}_2 \; .$$

Notice that, for convenience, we will frequently use a reference frame $(\vec{\zeta}_1, \vec{\zeta}_2, \vec{\zeta}_3)$ which is rotated with respect to $(\vec{b}_1, \vec{b}_2, \vec{b}_3)$. However we will use the notation g_1, g_2, g_3 for the components of $\vec{g}$ in the rotated frame as well.

The first of eq. (5) holds only for $g_1 = 0$, i.e. for a reciprocal lattice plane passing through the origin. (The case $g_1 \neq 0$ doesn't concern us, as it gives rise to a vanishingly small cross section). Under this assumption we have

$$q^2 = g_2^2 + g_3^2 \; ; \qquad Q_z = q_z E_o = \theta (g_2 \cos\alpha + g_3 \sin\alpha) \tag{7}$$

in which $\breve{\theta} = \theta / E_o$ is assumed to be small ($\sin\breve{\theta} \simeq \breve{\theta}$).

The condition $q_z \gtrsim \delta$ (or $\zeta \gtrsim 1$) is to be satisfied in performing the sum over $\vec{g}$ in eqs. (4) (remember the discussion on the pancake position in Sect. 2).

In eqs. (2), $I(x, E_o, \theta, \alpha)$ represents the so called bremsstrahlung intensity or spectrum of equivalent quanta; it is proportional to the energy radiated in the interval dk at k. It is broken up into two parts: I_i, which represents the interference contribution, and I_c, which is a continuous thermal background of the Bethe-Heitler type[9], as can be seen from eqs. (6). Strictly speaking, this continuous background can be classified as elastic. We can approximately include the contribution of inelastic processes which excite or ionize an atom (bremsstrahlung in the field of atomic electrons) multipliying $\psi^c_{1,2}$ by the factor $1 + \left[4 \cdot \ln(530\, Z^{-2/3})\right] / (Z \psi^c_1)$ (see ref. (9)).

I_i depends explicitly on x, E_o, θ and α, while χ_1 and χ_2 do not (they depend on α and on ratio only of θ/D). For a given θ/D and a given α, I_i is seen to depend linearly on $E_o/D = 1/\delta$ (eqs. (3)). This is a pretty nice scaling law; however $\breve{\theta} = \theta / E_o$ is decreased by increasing E_o, and this can give rise to experimental difficulties. In Fig. 3 we give an example of the functions $\chi_{1,2}(\theta/D, \alpha)$ obtained for Diamond with $\vec{\zeta}_1 = [110]$, $\vec{\zeta}_2 = [001]$, $\vec{\zeta}_3 = [1\bar{1}0]$, $\alpha = 0$. From these bremsstrahlung intensity of Fig. 2 is easily obtained; the dot-dashed curve represents the incoherent background of the Bethe-Heitler type, given by eqs. (6), while the dashed curve is the sum of the coherent plus incoherent contributions. In Sect. 7 details on the values of various numerical constants will be given.

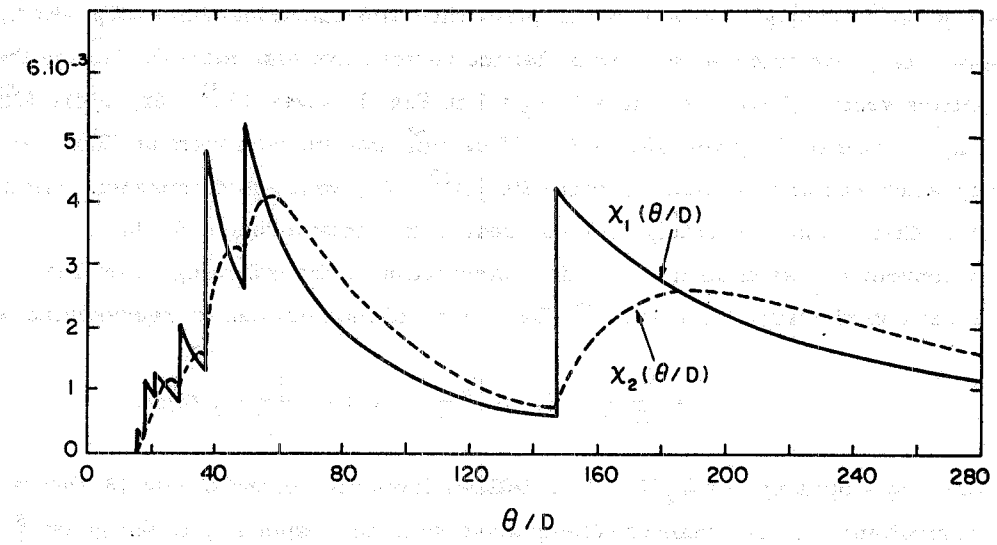

FIG. 3 - The functions $\chi_{1,2}(\theta/D, \alpha)$ versus $\theta/D, \alpha = 0$ for diamond. Axes as in Fig. 1.

The crystal properties enter the cross section through the term $\phi(\vec{g})$. Atomic properties are represented by $F(g^2)$; thermal properties by e^{-Ag^2} (A depends on the Debye as well as on the absolute temperature), crystal structure by the basis cell volume V and by the so called structure factor S (see eqs. (5)).

It is seen from eqs. (4) that each term of the sums is the product of a kinematical factor (that containing ξ) and an "intrinsic" factor $\phi(\vec{g})$. Thus the merit of the crystal can be judged by inspection of $\phi(\vec{g})$ only. Fig. 4 represents factors entering the first of eqs. (5).

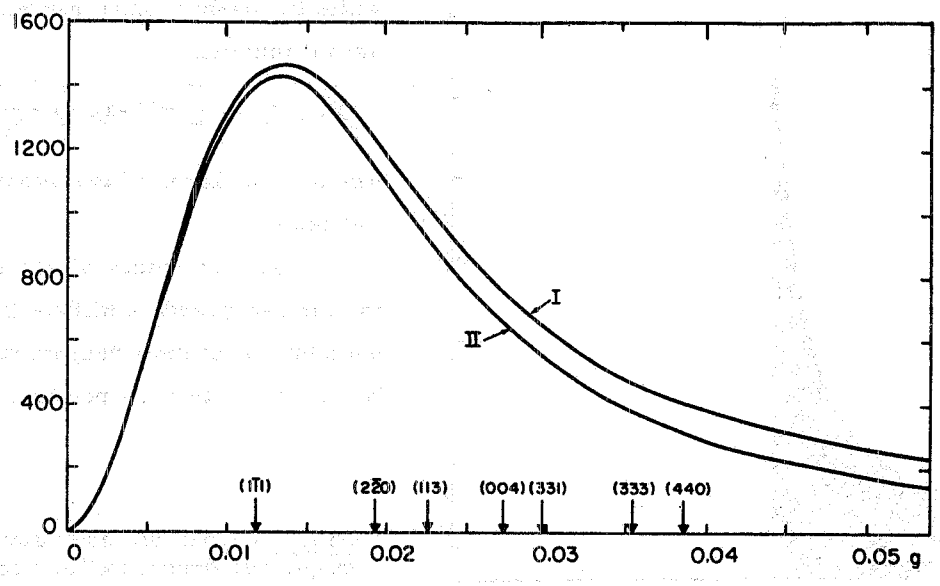

FIG. 4 - Curve I: $(1-F)^2/g^2$; curve II is curve I times $\exp(-Ag^2)$, versus g. See eqs. (5).

Curve I gives $(1-F)^2/g^2$ while curve II gives the same functions times $\exp(-Ag^2)$, versus g. The values of g for selected reciprocal lattice vectors are also marked. Notice that the reciprocal lattice vector $(1\bar{1}1)$ (i.e. : $n_2 = 1$, $n_3 = 1$ in Fig. 1) gives $|S|^2 = 32$, while $(2\bar{2}0)$ (i.e. : $n_2 = 0$, $n_3 = 2$ in Fig. 1) gives $|S|^2 = 64$. Thus $\phi(\vec{g})$ has its maximum at $(2\bar{2}0)$. In Fig. 1 circles represent reciprocal lattice points with $|S|^2 = 64$, while dots represent points with $|S|^2 = 32$. All other points are extinguished by destructive interference ($S = 0$).

A convenient way of looking at this factorization is the following. Consider I_i as the sum of different contributions from each $\vec{g}$. Each term of the sum can be represented by the equation

$$I_i^{\vec{g}} = \frac{E_o}{D}\left\{\left[1+(1-x)^2\right]\frac{1}{\xi^2} - 4(1-x)\,\frac{\xi-1}{\xi^4}\right\}\phi(\vec{g}) \,. \tag{8}$$

Now, by imposing $\xi = Q_z/D = 1$, it follows from the second of eqs. (3) that the position of the discontinuity in the bremsstrahlung spectrum, corresponding to the given $\vec{g}$ is

$$x_d = \frac{2Q_z}{1+2Q_z} \tag{9}$$

where Q_z is given by the second of eqs. (7). Eq. (8) can be written

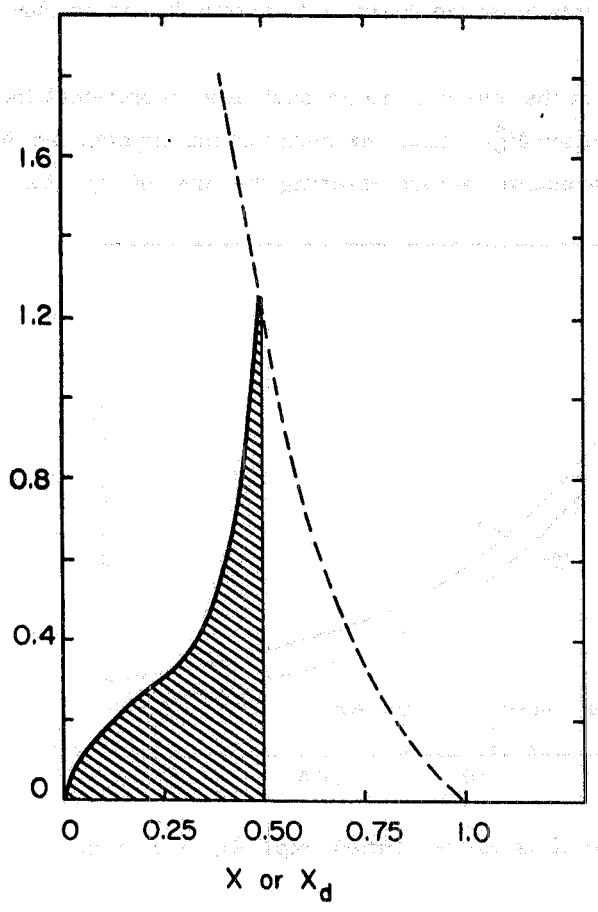

$$I_i^{\vec{g}}(x, x_d) = 2E_o\chi(x, x_d)\,\phi(\vec{g}) \tag{10}$$

which cleary exhibits all the previous properties. Fig. 5 shows the behaviour of the function $\chi(x, x_d)$ for $x_d = 0.5$ (shaded area), while the dashed curve represents the universal function

$$\chi(x_d, x_d) = \left[1+(1-x_d)^2\right]\frac{1-x_d}{x_d} \tag{11}$$

which is the locus of the maxima at the discontinuity.

Thus, by means of eqs. (10), (11) and (5) one can quickly estimate the coherent contribution of each reciprocal lattice point. Notice that, once the position of the first

FIG. 5 - Coherent contribution from a single reciprocal lattice vector $\chi(x, x_d)$, for $x_d = 0.5$ (shaded area), versus x. The dashed curve is $\chi(x_d, x_d)$, eq. (11), versus x_d.

discontinuity (the main one) has been chosen (see, for instance, Fig. 2), the position of the others are determined through eq. (9), taking into account that the possible Q_z's from eqs. (7) are all multiples of some minimum value. However only those values are present which are not extinguished by the structure factor S in eqs. (5).

Eq. (7) can also be solved for θ once the main x_d and α are given. Fig. 6 gives θ versus x_d for $\alpha = 0$, with the previous choice of $\vec{\zeta}_1$, $\vec{\zeta}_2$, $\vec{\zeta}_3$ for Diamond.

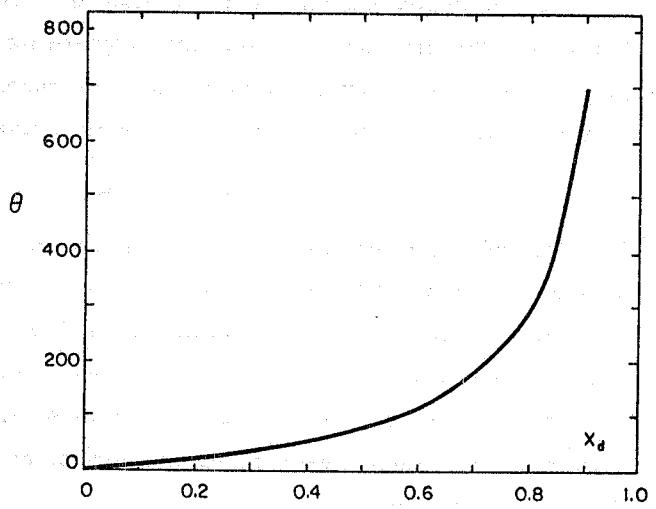

FIG. 6 - θ versus x_d, $\alpha = 0$ for diamond, axes as in Fig. 1.

4. - VALIDITY OF THE BORN APPROXIMATION

For a sufficiently high E_o and/or sufficiently low θ, there will be some value of δ for which the bremsstrahlung cross section will be higher than the geometrical cross section of the atom, and this is manifestly absurd. The failure to predict the exact value of the cross section is connected with the non validity of the Born approximation in certain conditions. A careful nalaysis of this problem has been done in a series of papers by Akhiezer and collaborators (see ref. (12) and references cited therein). The results of this analysis are the following.

The results of the calculations obtained by applying the first Born approximation are valid when

$$\frac{Z}{137}\,\frac{1}{2\pi a\theta} \ll 1 .$$

When this inequality is not satisfied, the coherent nature of the bremsstrahlung is lost, and the radiation is suppressed. This happens for diamond for

$$\breve{\theta} \simeq 5 \times 10^{-5} \text{ rad.}$$

Furthermore the bremsstrahlung intensity depends on the sign of the charge of the particle (larger for electrons than for positrons). The critical parameter in this context is

$$\frac{Z}{137}\,\frac{E_o}{\theta^2}\,\frac{1}{2\pi a} .$$

When this parameter is comparable to 1, a new phenomenon arises: the so called axial channeling.

In a standard experimental situation the primary beam divergence will be of the order of 0.5 mrad. We can thus state that the suppression effect should be negligible. Equally, at very high energy, the radiation emission in axial channeling condition can hardly be observed. For instance, for $\check{E}_o$ = 100 GeV the characteristic angle for axial channeling for diamond would be

$$\check{\theta} = 2 \times 10^{-5} \text{ rad.}$$

The critical angle for planar channeling is even less than this (it is multiplied by β/a, where β is the screening ratio of the atom (see eq. (6)).

In conclusion we can be confident that Born approximation calculations can be used at least for low Z and not too high particle energies, if the primary beam angular divergence is not too small. Also, the difference in bremsstrahlung between electron and positron should be negligible. For these reasons, all the results presented in this paper were calculated in first Born approximation.

5. - EFFECTS OF EXPERIMENTAL RESOLUTIONS

The formulae given so far can't be used as such in practice. There are sources of experimental imperfections which tend to smear the coherence effect. Among these sources we can include:

(a) multiple scattering of primary electrons in the crystal;

(b) intrinsic divergence of the primary electron beam;

(c) mosaic structure of the crystal;

(d) mechanical vibration of the goniometer holding the crystal.

Effect (a) is represented by an exponential-integral angular density distribution, while (b) and (c) can be globally represented by a gaussian density distribution whose variance is obtained by summing the variances for each effect.

This approach has been considered in ref. (11). However the angular distribution density used had a circular symmetry around the primary electron beam axis, and so isn't suitable to represent beams with different sizes in the horizontal and vertical direction.

As we are specifically interested in this beam feature (see Sect. 7) we now expalin how the final cross section has been obtained. First of all, at the energies we are interested in ($\check{E}_o \sim 100$ GeV), effect (a) is completely negligible with respect to (b), at least for a moderate crystal thickness. So we do not consider it any further.

Let $\vec{p}_o^{\,*}$ be the central momentum of the primary electron beam. The actual electron momentum $\vec{p}_o$ is specified by the polar angle $\omega = \sphericalangle(\vec{p}_o^{\,*}, \vec{p}_o)$ and the azimuthal angle $\varphi = \sphericalangle(\vec{p}_o^{\,*}, \vec{p}_o)(\vec{p}_o, \vec{\zeta}_1)$. Like $\check{\theta}$, $\check{\omega} = \omega/E_o$ is assumed to be small ($\sin\check{\omega} \simeq \check{\omega}$). The new definitions for θ and α are:

$$\theta = \sphericalangle(\vec{\zeta}_1, \vec{p}_o^{\,*}) \; ; \qquad \alpha = \sphericalangle(\vec{\zeta}_1, \vec{p}_o^{\,*})(\vec{\zeta}_1, \vec{\zeta}_2) \tag{12}$$

and Q_z in eqs. (7) shall be replaced by

$$Q_z = \theta \left[g_2 \cos\alpha + g_3 \sin\alpha \right] - \omega \left[g_2 \cos(\alpha - \varphi) + g_3 \sin(\alpha - \varphi) \right] . \qquad (13)$$

The bremsstrahlung intensity in eqs. (3) is now folded with the appropriate angular distribution density $G(\omega, \varphi)$:

$$\int_0^{2\pi} d\varphi \int_0^{\infty} I_i(x, E_o, \theta, \alpha, \omega, \varphi)\, G(\omega, \varphi)\, \omega\, d\omega . \qquad (14)$$

We assumed for $G(\omega, \varphi)$ a bivariate normalized gaussian function

$$G(\omega, \varphi) = \frac{1}{2\pi \omega_H \omega_V} \exp - \left(\frac{\omega^2}{2\omega_H^2} \cos^2\varphi + \frac{\omega^2}{2\omega_V^2} \sin^2\varphi \right) , \qquad (15)$$

where ω_H and ω_V represent the standard deviations of the angular divergence in the horizontal and vertical plane, respectively (assumed to be uncorrelated). As an example, we can assume

$$\omega_H = (\omega_{DH}^2 + \omega_M^2)^{1/2} , \qquad \omega_V = (\omega_{DV}^2 + \omega_M^2)^{1/2} , \qquad (16)$$

where ω_{DH} and ω_{DV} are the standard deviations of the primary electron beam divergence in the horizontal and vertical plane, respectively, and ω_M is the standard deviation of the $\vec{\zeta}_1$ axis mosaic spread (assumed to be circularly symmetric).

More complex combinations can be envisaged to include mechanical vibrations and possibly other effects.

The integration in eq. (14) will of course be performed numerically. Owing to the discontinuous nature of the function I_i, the integration gives awkward results if ω_H, ω_V are comparable with $\theta_H = \theta \cos\alpha$ and $\theta_V = \theta \sin\alpha$, respectively.

6. - CHOICE OF BEST CRYSTAL

We already mentioned in Sect. 3 that the merit of a crystal can be judged by looking at the bahaviour of $\phi(\vec{g})$. Numerical values of the atomic form factors $F(q^2)$ have been obtained from expressions of the form

$$F(q^2) = \sum_{i=1}^{4} \alpha_i \exp(-\beta_i q^2) + c . \qquad (17)$$

A systematic tabulation of the coefficients α_i, β_i and c for all Z exists[13].

In eqs. (5) the maximum value of $|S|^2/n$ is clearly n, the number of atoms in the basis cell. Thus we define the merit factor of the crystal by

$$M = \frac{n}{V} \left\{ \frac{\left[1 - F(g^2) \right]^2}{g^2} \right\} \text{Max} \qquad (18)$$

TABLE I - Merit factor of selected crystals (eq. (18)).

Element	Z	Structure type(*)	n	Lattice constants (Å & deg.)	$\check{V}_o$ $(Å)^3$	$\frac{(1-F)^2}{g^2}_{MAX}$	$\check{M}$
Li	3	b.c.c.	2	3.51	43.2	2727	126
Be	4	h.c.p.	2	2.29; 3.58	16.3	2667	326
B α	5	rhomb.	12	5.06;58.10°	87.4	2124	292
C(diamond)	6	diam.	8	3.57	45.5	1462	257
C(graphite)	6	hexagonal	4	2.46; 6.71	35.2	1462	166
Na	11	b.c.c.	2	4.29	79.0	625	16
Mg	12	h.c.p.	2	3.21; 5.21	46.5	761	33
Al	13	f.c.c.	4	4.05	66.4	882	53
Si	14	diam	8	5.43	160.1	936	47
Ti	22	h.c.p.	2	2.95; 4.69	35.3	724	41
Fe α	26	b.c.c.	2	2.87	23.6	563	48
Co α	27	h.c.p.	2	2.51; 4.07	22.2	529	48
Ni	28	f.c.c.	4	3.52	43.6	498	46
Cu	29	f.c.c.	4	3.62	47.4	464	39
Zn	30	h.c.p.	2	2.66; 4.93	30.2	443	29
Ge	32	diam	8	5.66	181.3	424	19
Mo	42	f.c.c.	4	4.16	72.0	470	26
Rh	45	f.c.c.	4	3.80	54.9	453	33
Ag	47	f.c.c.	4	4.09	68.4	436	25
Sn α	50	diam	8	6.49	273.4	418	12
Ta	73	b.c.c.	2	3.31	36.3	289	16
W	74	b.c.c.	2	3.17	31.9	288	18
Ir	77	f.c.c.	4	3.84	56.6	287	20
Pt	78	f.c.c.	4	3.92	60.2	287	19
Au	79	f.c.c.	4	4.08	67.9	287	17
Tl α	81	h.c.p.	2	3.45; 5.51	56.8	285	10
Pb	82	f.c.c.	4	4.95	121.3	284	9
Be_2B	4,5	CaF_2	12	4.66	101.2	2667	316
Be_2C	4,6	CaF_2	12	4.34	81.7	2667	392
B_4C	5,6	rhomb.	15	5.17;65.5°	112.0	2124	284

(*) f.c.c. = face centered cubic
b.c.c. = base centered cubic
h.c.p. = hexagonal closest packing
diam. = diamond
rhomb. = rhombohedral
CaF_2 = CaF_2 cubic type

where the maximum value is to be calculated with respect to g^2. Apart from a multiplicative factor, it represents the upper bound of $\phi(\vec{g})$. The best crystals should be those for which M is largest.

Of course it is not guaranted that the maximum of $|S|^2$ be combined with the maximum of $(1-F)^2/g^2$ (remember what has been said in Sect. 3 regarding Fig. 4). M should be considered only a rough parameter which exhibits the general trend of crystals of the elements with respect to coherent bremsstrahlung. For this reason it isn't worth improving M. For instance, multiplication by $\exp(-Ag^2)$ and division by ψ_1^c is not performed.

Table I shows M versus Z for a selection of element crystals. The various factors affecting M are also shown. The conclusion is very clear: low-Z crystals are the best ones, essentially because $(1-F)^2/g^2$ is largest. The group with Z between 3 and 6 is by far the best. Then comes the group with Z between 13 and 30, but with much smaller M. Other Z's are not attractive.

At this point M has accomplished its role. It is now time to look at finer details for the best crystals. We have chosen three crystals (Beryllium, Boron and Diamond) as representative of the first group and Silicon as representative of the second group.

In order to evaluate exactly the performance of these crystals we have to compute $\phi(\vec{g})$ for all the relevant lattice vectors and choose the largest value for each crystal. The ratio

$$P = \frac{\phi(\vec{g})_{Max}}{\psi_1^c} \qquad (19)$$

can be considered as the performance parameter. The results are summarized in Table II, where we give $P/P_{Diamond}$ for the four crystals.

The conclusion is that Beryllium is slightly worse than Diamond (while from Table I it appeared slightly better). This statement had already been made in ref. (11). Performance of Boron and Silicon is worse. Thus Beryllium and Diamond are almost equivalent, and can hardly be rivalled by other crystals of the elements as far as coherent bremsstrahlung is concerned.

TABLE II - Performance parameter $P/P_{Diamond}$ (eq. (19)).

Crystal	Best Reciprocal Vector	$\frac{P}{P_{Diamond}}$
Diamond	$22\bar{0}$	1.00
Beryllium	002	0.86
Boron	208	0.38
Silicon	$22\bar{0}$	0.19
Be_2C	220	1.10

Between Beryllium and Diamond we definitely prefer Diamond, which has been used extensively in the past years for coherent bremsstrahlung production. Almost perfect crystals can be found, which match the required mosaic spread standard deviation ($< \sim 0.1$ mrad). The only disadvantage is the high price.

On the other hand Beryllium lacks any experimental test in our field of interest. Defect free single crystals with the required limit on mosaic spread are difficult to manufacture. We will insist on this solution only if the funding of Diamonds is impossible.

Compound crystals could also be investigated. This search should be restricted to low-Z as well. All this will be matter for a future work, but just to give some impression of the situation, merit factors, still defined by eq. (18), are added at the end of Table I for beryllium boride, beryllium carbide and boron carbide. Beryllium carbide seems very promissing: it has the largest merit factor in the Table. So the performance parameter for this crystal, equivalent to eq. (19), has been computed and added at the end of Table II. It is confirmed that Be_2C shouls be even better than Diamond.

7. - NUMERICAL RESULTS AND PRACTICAL CONSIDERATIONS FOR DIAMOND

The importance of using an accurate value for the atomic form factor has been pointed out in ref. (10). So, for Diamond we haven't used in eq. (17) the parameters tabulated in ref. (13). Instead, we exploited the form factor and the A-value which have been experimentally determined by an X-ray scattering experiment[14]. We performed a non linear least square fit of $F(q^2)$ by means of eq. (17) and obtained the following parameters

$$Z\alpha_1 = 2.19835 \qquad \beta_1 = 6612.50$$
$$Z\alpha_2 = 1.97977 \qquad \beta_2 = 6630.08$$
$$Z\alpha_3 = 1.69080 \qquad \beta_3 = 176.49$$
$$Z\alpha_4 = 1.17186 \qquad \beta_4 = 47745.6$$
$$Zc = 0.01400$$

The sum of the $Z\alpha_i$ and Zc doesn't equal 6 as it should be, because experimental points are missing[14] for $q \to 0$. However the least-square fit-determined F(q) is in agreement with the experimental values in the relevant range within the measurement errors. Other parameters for cubic diamond at room temperature are

$$a_1 = a_2 = a_3 = a = 146.7 \; ; \quad A = 170.0 \; ; \quad \psi_1^c = 14.6 \; ; \quad \psi_1^{BH} = 18.4 \quad \text{(see eqs. (24))} \; ;$$

$n = 8$; u_{1_j}, u_{2_j}, u_{3_j} are

$$0\,0\,0 \; ; \; \tfrac{1}{2}\,\tfrac{1}{2}\,0 \; ; \; \tfrac{1}{2}\,0\,\tfrac{1}{2} \; ; \; 0\,\tfrac{1}{2}\,\tfrac{1}{2} \; ; \; \tfrac{1}{4}\,\tfrac{1}{4}\,\tfrac{1}{4} \; ; \; \tfrac{1}{4}\,\tfrac{3}{4}\,\tfrac{3}{4} \; ; \; \tfrac{3}{4}\,\tfrac{1}{4}\,\tfrac{3}{4} \; ; \; \tfrac{3}{4}\,\tfrac{3}{4}\,\tfrac{1}{4} \; .$$

Reference axes have been chosen as indicated in Fig. 1 :

$$\vec{\xi}_1 = [1\bar{1}0]; \quad \vec{\xi}_2 = [001] \; ; \quad \vec{\xi}_3 = [1\bar{1}0] \; ; \quad \vec{g}_1 = 0 \; ; \quad g_2 = \frac{n_2}{a} \; ; \quad g_3 = \sqrt{2}\,\frac{n_3}{a} \; . \qquad (20)$$

The integers n_2, n_3 (see Fig. 1) are allowed to span sufficiently the abscissa in Fig. 4 to reach $\phi(\vec{g})$ values smaller than $0.05\,\phi_{MAX}$ ($n_2 = 0$, $n_3 = 2$).

Our main interest is to catch $(2\bar{2}0)$, the best $\vec{g}$ (see Table II), within the kinematical pancake.

As an example, assume the diamond is mounted onto the two rotation axes (horizontal and vertical) of a goniometer, in such a way that the axes $\vec{\zeta}_2$ and $\vec{\zeta}_3$ are parallel to the horizontal and vertical axes respectively. Let us call θ_H (θ_V) the angle of rotation in the horizontal (vertical) plane, i.e. : around the vertical (horizontal) axis.

In the small polar angle approximation we are systematically using, we can write

$$\theta_H = \theta \cos\alpha \; ; \quad \theta_V = \theta \sin\alpha \; ; \quad \frac{\theta_H}{\theta_V} = \mathrm{ctg}\,\alpha \; ; \quad \theta_H^2 + \theta_V^2 = \theta^2 \; ; \quad Q_z = g_2\theta_H + g_3\theta_V \; . \tag{21}$$

In particular, for the $(2\bar{2}0)$ vector we have $n_2 = 0$, $n_3 = 2$, and

$$Q_z = g_3\theta_V = \frac{2\sqrt{2}}{a}\,\theta_V \; . \tag{22}$$

If we want the discontinuity position at value x_d in the spectrum, the condition $Q_z > D$ gives us

$$\theta_V = \frac{1}{E_o}\,\frac{a}{4\sqrt{2}}\,\frac{x_d}{1-x_d} \text{ rad} \; .$$

A typical SPS electron energy is $\check{E}_o = 150$ GeV. Thus

$$\check{\theta}_V = 8.83 \times 10^{-5}\,\frac{x_d}{1-x_d} \; ; \quad \frac{d\theta_V}{\theta_V} = \frac{x_d}{1-x_d}\,\frac{dx_d}{x_d} \; . \tag{23}$$

This gives $\check{\theta}_V = 0.35$ mrad for $x_d = 0.8$ and $\check{\theta}_V = 0.80$ mrad for $x_d = 0.9$. Furthermore x_d is insensitive to variations of θ_V for $x_d \to 1$. A change of 0.1 mrad in $\check{\theta}_V$ changes $x_d = 0.9$ by only 0.01. Thus 0.1 mrad is the ultimate goniometer sensitivity needed. Having specified θ_V, θ_H can be chosen at will, still preserving the position of the discontinuity (this is so only because $n_2 = 0$). Thus $\check{\theta}_H$ shall be taken as large as several mrad ($\theta_H \gg \theta_V$).

The orientation procedure consists essentially in turning the crystal around the axis $[1\bar{1}0]$ by a "large" angle and then tilting it a little bit around the axis $[001]$. In effect it isn't necessary that these axes be exactly aligned along the goniometer rotation axes. The bremsstrahlung detection procedure itself is capable of determining the exact axis position, thus allowing for the appropriate corrections to the angles.

This way of orienting the crystal has already been used[10] to improve the linear polarization of the beam. The fact that only one of the goniometer rotations is required to be small can be exploited to improve the photon flux as well[5,7]. In effect the horizontal and vertical divergences of the primary electron beam are constrained to be sufficiently smaller than θ_H and θ_V, respectively. So, in the previous example only the vertical divergence must be very small (~ 0.1 mrad). The horizontal divergence can be as large as some mrad. Thus the primary beam transport system has to perform a sharp collimation only in the vertical direction. In this way the electron (and thus the photon) flux can be higher than the flux obtainable when both collimations are sharp.

Given a fixed electron beam vertical emittance, small vertical divergence means large vertical beam spot size. The beam spot will thus be elongated in the vertical direction. If for any reason only a spot elongated in the horizontal direction is tolerated, one has only to exchange the role of θ_H and θ_V: $[1\bar{1}0]$ should be placed horizontal and $[00\bar{1}]$ vertical.

One is not necessarily bound to exploit the "best" vector $(2\bar{2}0)$. Also (220), (022), etc. perform equally well the job, inasmuch as they all have the same $F(g^2)$ and S (see eqs. (5)). This allows orienting the crystal along axes different from $[110]$.

We think that all these predictions must have the support of a quantitative evaluation. For this reason we have performed detailed computations by folding the bremsstrahlung cross section with the angular distribution given by eq. (15). Effects of different horizontal and vertical divergences have thus been numerically investigated. Results of computations are summarized in Figs. 7 and 8.

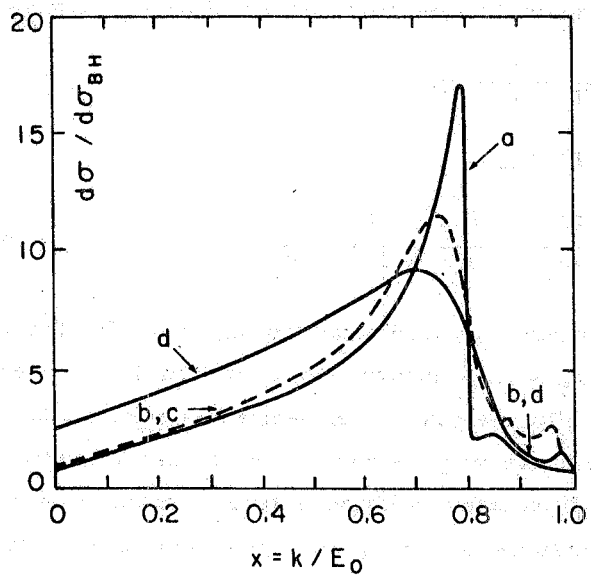

FIG. 7 - Ratio of the coherent plus incoherent cross section to the Bethe-Heitler cross section, versus $x=k/E_o$, $x_d = 0.80$; $\breve{\theta}_V = 0.35$ mrad;
a: $\breve{\omega}_H = \breve{\omega}_V = 7 \times 10^{-6}$ rad; $\breve{\theta}_H = 57.8$ mrad; $\alpha = 0.35^o$.
b: $\breve{\omega}_H = 0.7$ mrad; $\breve{\omega}_V = 0.07$ mrad; $\breve{\theta}_V =$ = 20.2 mrad; $\alpha = 1^o$.
c: $\breve{\omega}_H$, $\breve{\omega}_V$ same as in Fig. 7, curve b; $\breve{\theta}_H = 10.1$ mrad; $\alpha = 2^o$.
d: ω_H, θ_H same as in Fig. 7, curve b; $\breve{\omega}_V = 0.15$ mrad.

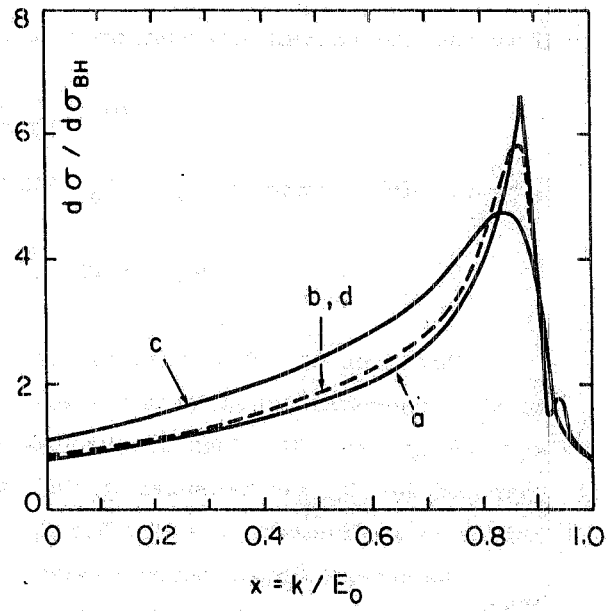

FIG. 8 - Same ratio as in Fig. 7. $x_d = 0.9$; $\breve{\theta}_V = 0.80$ mrad; $\breve{\theta}_H = 45.6$ mrad; $\alpha = 1^o$.
a: ω_H, ω_V same as in Fig. 7, curve a.
b: $\breve{\omega}_V = 0.15$ mrad; $\breve{\omega}_H = 0.7$ mrad.
c: $\breve{\omega}_V = 0.3$ mrad; $\breve{\omega}_H = 0.7$ mrad.
d: ω_V same as in Fig. 8, curve b; $\breve{\omega}_H = 3.5$ mrad.

Here we present the gain ratio $d\sigma/d\sigma_{BH}$, where $d\sigma$ corresponds to eqs. (2)-(6), (13)-(15) and $d\sigma_{BH}$ is the complete streening Bethe-Heitler cross section, valid for non-crystal material[9], given by

$$d\sigma_{BH} = \bar{\sigma}\,\frac{dx}{x}\left\{\left[1+(1-x)^2\right]\psi_1^{BH} - \frac{2}{3}(1-x)\psi_2^{BH}\right\};$$
$$\psi_1^{BH} = 4\ln(183\,Z^{-1/3}); \qquad \psi_2^{BH} = \psi_1^{BH} - \frac{2}{3}, \tag{24}$$

where $\bar{\sigma}$ is the same as in eqs. (2). The abscissa is the photon fractional energy $x = k/E_o$. The electron energy is $\check{E}_o = 150$ GeV. Crystal axes have been chosen as in eqs. (20).

The detailed features of the figures are the following:

Fig. 7 : $x_d = 0.8$; $\check{\theta}_V = 0.35$ mrad

Curve a : $\check{\omega}_H = \check{\omega}_V = 7 \times 10^{-6}$ rad ; $\check{\theta}_H = 57.8$ mrad ; $\alpha = 0.35^o$.

This curve is given to show the best which can be obtained with a perfect electron beam (no divergence) and a perfect diamond crystal (no mosaic spread). Multiple scattering is the only allowed smearing effect. The given value of ω_H, ω_V simulate approximately the multiple scattering in a 3 mm thick diamond crystal. A gain of a factor $\sim$16 is obtained at the principal maximum at $x_d = 0.8$. Secondary maxima are much smaller.

Curve b : $\check{\omega}_H = 0.7$ mrad ; $\check{\omega}_V = 0.07$ mrad $= 0.2\,\check{\theta}_V$; $\check{\theta}_H = 20.2$ mrad ; $\alpha = 1^o$.

Curve c : ω_H, ω_V same as for curve b ; $\check{\theta}_H = 10.1$ mrad ; $\alpha = 2^o$.

Now ω_H, ω_V represent electron beam divergences as well as crystal mosaic spread, dominating multiple scattering. The gain at the maximum is decreased to 12 and the slope of the curve around $x_d = 0.8$ is less than for curve a. This is mainly due to the vertical standard deviation ω_V which is one fifth of θ_V. The two curves are coincident, except at secondary maxima, thus showing the expected independency of θ_H. This is true of course only in the limit that ω_V is sufficiently smaller than θ_V (1/20 and 1/10 for curves b and c, respectively).

Curve d : ω_H, θ_H, α same as for curve b ; $\check{\omega}_V = 0.15$ mrad $\simeq 0.4\,\check{\theta}_V$.

The general trends of curves b, c are more accentuated. The gain factor at the maximum is decreased to 9, and the curve is, loosely speaking, broader than curves b, c by a factor of 2. What is worse in this case is that a gain of a factor ~ 3 is obtained on soft photons as well. The "effective" gain is only a factor 3.

The general conclusion on these curves is that a gain of a factor > 10 can be obtained at $x_d = 0.80$ only if the vertical standard deviation $\check{\omega}_V$ is smaller than 0.1 mrad, a very small angle indeed.

Fig. 8 : $x_d = 0.9$; $\check{\theta}_V = 0.8$ mrad ; $\check{\theta}_H = 45.6$ mrad ; $\alpha = 1^o$

Curve a : ω_H, ω_V same as Fig. 7, curve a.

This is the best curve for $x_d = 0.9$. The gain at the maximum is ~ 7, which had to be expected from Fig. 7 curve a, on the basis of the scaling law (see Sect. 3).

Curve b : $\breve{\omega}_V = 0.15$ mrad $\simeq 0.2\ \breve{\theta}_V$; $\breve{\omega}_H = 0.7$ mrad.

Curve c : $\breve{\omega}_V = 0.3$ mrad $\simeq 0.4\ \breve{\theta}_V$; $\breve{\omega}_H = 0.7$ mrad.

These two curves have about the same ω_V/θ_V ratio as curves b and d in Fig. 7, respectively. In this case the curves are less sensitive to the increase in ω_V/θ_V. This had to be expected on the basis of the second of eqs. (23). Differently from curve d in Fig. 7, there is no substantial soft photon production for curve c and the "effective" gain is about 5 instead of 3.

Curve d : ω_V same as for curve b ; $\breve{\omega}_H = 3.5$ mrad.

This is almost coincident with curve b and is presented with the aim of showing how large a divergence is tolerated in the horizontal plane. In effect it could be even larger, provided that it is sufficiently smaller than $\breve{\theta}_H = 45.6$ mrad.

Finally we report in Fig. 9 the ratio $d\sigma/d\sigma_{BH}$ computed for Silicon in the same conditions as Fig. 8, curve a, except that now we obtain $\breve{\theta}_V = 1.21$ mrad, $\breve{\theta}_H = 69.4$ mrad. It is shown for comparison just to give the visual impression of how much is lost by using silicon in place of diamond. The loss factor is about 3, i.e., better than predicted by Table II on the basis of the best reciprocal vector only (loss factor of about 5). In fact contributions due to all relevant reciprocal vectors are included in Fig. 9.

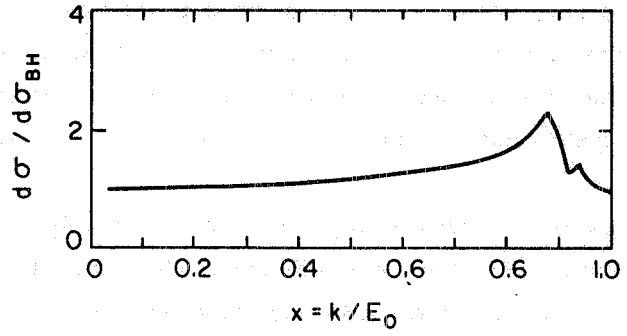

FIG. 9 - Same as Fig. 8, curve a, but for Silicon ; $\breve{\theta}_V = 1.21$ mrad ; $\breve{\theta}_H = 69.4$ mrad.

As a conclusion we can say that, of all cases considered, the most realistic results obtained are curves b and c in Fig. 8.

One must be aware that the beam is polarized, because this can have important consequences in the experimental utilization. However it results from our computation that the polarization is rather small : less than 30 % in all cases with $x_d = 0.8$ and less than 15 % in all cases with $x_d = 0.9$.

8. - CONCLUDING REMARKS

It is interesting to compare the performances of the coherent beam with the normal bremsstrahlung beam. We consider a typical coherent photoproduction process from nuclei in which the cross section is negligible below 40 GeV, increases linearly up to 80 GeV and then reaches a flat top: Fig. 10 gives in arbitrary units the number of particles with mass between 3.6 and 4.6 GeV coherently photoproduced from a Silicon target, versus photon energy. Curve a was obtained for the normal bremsstrahlung beam used so far in the NA1 experiment[1], while curves b and c were obtained by using the results of Fig. 8, curves b and c, respectively. The curves are normalized to the same number of incident electrons.

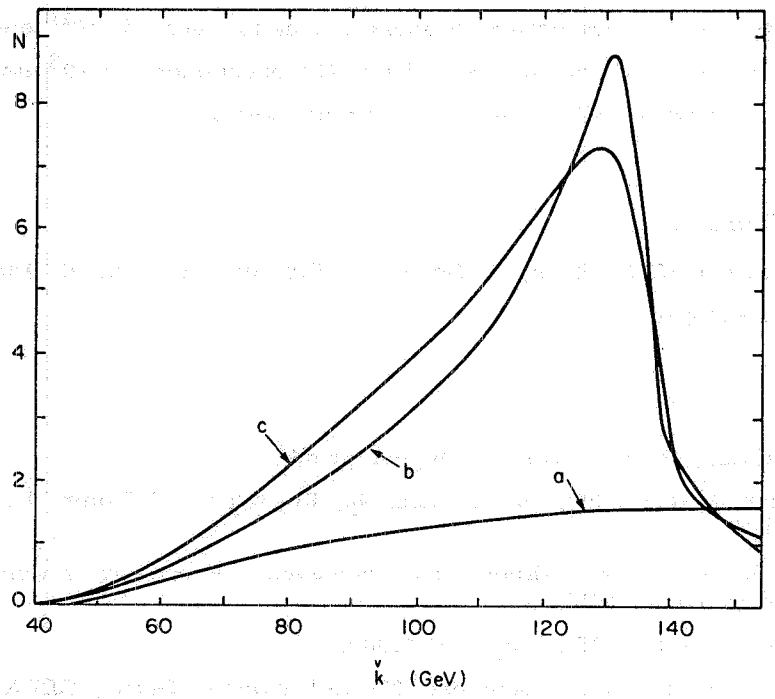

FIG. 10 - N is the number of particles with mass between 3.6 and 4.6 GeV coherently photoproduced from a Silicon target, versus photon energy k (arbitrary units). Curve a is obtained for a normal bremsstrahlung beam. Curves b and c are obtained by using coherent bremsstrahlung spectra of Fig. 8b and 8c, respectively. The curves are normalized to the same number of incident electrons.

If n_a, n_b, n_c are the total number of particles photoproduced between 40 and 150 GeV for curves a, b, c, respectively, one obtains

$$n_a : n_b : n_c = 1 : 2.8 : 3.1 .$$

Thus the oriented diamond crystal should provide us with a mean of increasing the photoproduction rate by a factor of ~ 3 with respect to the case of an unoriented material of the same thickness (in R.L.), without increasing substantially the soft photon production. In effect

it is just the multiple emission of soft photons which presently prevents the photon tagging system[1] from being operated with a radiator thickness larger than 0.1 R.L..

Whether the coherent beam we have considered could be in practice utilized in Experiment NA1 or not depends critically on the required size of the diamond. If we want a photoproduction rate of a factor of ~ 3 with respect to the present one (obtained with a radiator 0.1 R.L. thick), the thickness of the diamond should be $0.1 \cdot 122 = 12$ mm. If this is considered as the point-to-point distance in the diamond octohedron, the edge size is $12/\sqrt{2} = 8.5$ mm, and the diamond weight is $(1/3)\,(12^3/\sqrt{2})\,3.5\times10^{-3} = 1$ gr. Several of these diamonds can be oriented at the same angle to cover the beam spot size.

As far as the ageing of diamond is concerned, one has to consider the process of atom dislocation due to electron irradiation. A useful life up to a dose of $\sim 10^{20}$ electrons/cm^2 has been estimated. In terms of typical fluxes of the NA1 experiment ($\sim 10^6$ electrons/cm^2 burst)), this means $\sim 10^{14}$ burst or $\sim 10^{15}$ sec, i.e. : almost eternity !

ACKNOWLEDGMENTS

Discussions with G.A. Beck, N. Doble, F. Fidecaro, L. Foà, D. Plane and L. Rolandi are greatly acknowledged.

REFERENCES

(1) - E. Albini et al., Phys. Letters (to be published).

(2) - G. Diambrini Palazzi, Rev. Mod. Phys. 40, 611 (1969); U. Timm, Fort. d. Phys. 17, 765 (1969).

(3) - M. L. Ter-Mikaelian, High-Energy Electromagnetic Processes in Condensed Media (Wiley-Interscience, 1972).

(4) - V. A. Maisheev et al., JETP 50, 856 (1980).

(5) - G. Diambrini Palazzi and A. Santroni, 300 GeV Working Group, CERN/ECFA/72/4, Vol. I, Page 231; See also G. Diambrini Palazzi, E. Menichetti and A. Santroni, Nuclear Instr. 126, 369 (1974).

(6) - G. Bologna, F. Celani, B. D'Ettorre Piazzoli, G. Mannocchi and P. Picchi, Proceedings of the Meeting on Miniaturization of High Energy Physics Detectors, Pisa 1980.

(7) - M. J. Tannenbaum, Report BNL-28586; Presented at 1980 Symposium on High Energy Physics with Polarized Beams and Polarized Targets, Lausanne 1980.

(8) - R. Del Fabbro and G. P. Murtas, Phys. Scripta 23, 690 (1981); Presented at the Intern. Conf. on Experimentation at LEP, Uppsala 1980.

(9) - H. W. Koch and J. W. Motz, Rev. Mod. Phys. 31, 920 (1959).

(10) - G. Bologna, G. Lutz, H. D. Schulz, U. Timm and W. Zimmerman, Nuovo Cimento 42A, 844 (1966).

(11) - G. Bologna, Nuovo Cimento 49A, 756 (1967); Errata 50A, 678 (1967).

(12) - A. I. Akiezer, V. F. Boldishev and N. F. Shul'ga, Sov. J. Part. Nucl. 10, 19 (1979).

(13) - D. T. Cromer and J. T. Waber, Acta Cryst. 18, 104 (1965); 19, 224 (1965).

(14) - S. Gottlicher and E. Wölfel, Zeits. f. Elektrochemie 63, 891 (1959).